Latest Results from the Search for $K^+ \to \pi^+ \nu\bar{\nu}$

Joe Mildenberger[a*]

[a]TRIUMF, 4004 Wesbrook Mall, Vancouver, British Columbia, Canada, v6t 2a3

Brookhaven experiment E949 has continued the search for the rare decay $K^+ \to \pi^+ \nu\bar{\nu}$. The branching ratio for this second-order weak transition is an important test of the Standard Model; deviations from the predicted branching ratio of $\sim 0.8 \times 10^{-10}$ could be indications of non-Standard Model physics. While the Standard Model prediction for the branching ratio has a small ($\sim 7\%$) theoretical uncertainty, the experimental and analytical hurdles involved in making this measurement are formidable. This paper describes the key features of some of the techniques used in the measurement of $\mathcal{B}(K^+ \to \pi^+ \nu\bar{\nu})$.

1. Introduction

In the 3-generation Standard Model the flavour-changing neutral currents responsible for the $K^+ \to \pi^+ \nu\bar{\nu}$ decay proceed via 2$^{\text{nd}}$-order transitions (Fig. 1).

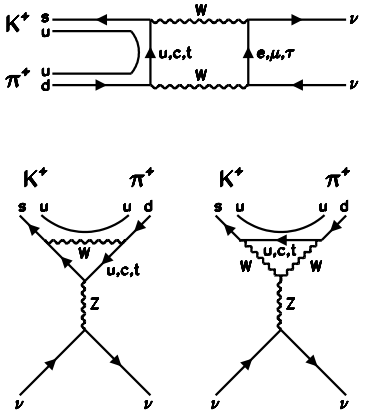

Figure 1. Second-order weak transitions responsible for the $K^+ \to \pi^+ \nu\bar{\nu}$ decay.

Using the Wolfenstein parametrization[1] to represent the quark couplings specified by the Cabibbo-Kobayashi-Maskawa matrix

$$U = \begin{pmatrix} V_{ud} & V_{us} & V_{ub} \\ V_{cd} & V_{cs} & V_{cb} \\ V_{td} & V_{ts} & V_{tb} \end{pmatrix} = \begin{pmatrix} 1-\frac{1}{2}\lambda^2 & \lambda & A\lambda^3(\rho - i\eta) \\ -\lambda & 1-\frac{1}{2}\lambda^2 & A\lambda^2 \\ A\lambda^3(1-\rho-i\eta) & -A\lambda^2 & 1 \end{pmatrix}$$

where $\lambda \equiv V_{us} = \sin\theta_c$, the sine of the Cabibbo angle, and imposing the constraint of unitarity allows the relationships between the matrix elements to be represented as a unitarity trinagle in the complex plane. Thus, the consistency of the

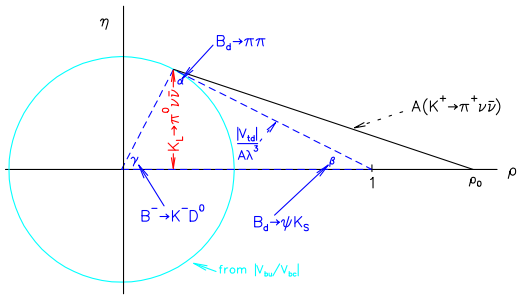

Figure 2. Unitarity triangle in the $\rho - \eta$ plane

measured quantities corresponding to the sides and angles of the triangle consititutes a crucial test of the ability of the Standard Model to correctly described weak interactions.

Of the measurements which can be used to specify the unitarity triangle shown in Fig. 2 there are four that can be calculated with small theoretical uncertainties:

- $\mathcal{A}(B \to J/\psi K^0_S; t)$, the time-dependent, CP-violating decay rate asymmetry, measured at B-factories by the BaBar and Belle collaborations

*On behalf of the E949 Collaboration

- $\Delta m_s/\Delta m_d$, the ratio of "mixing" frequencies of neutral B mesons, measured at Fermilab by the CDF and D0 collaborations
- $\mathcal{B}(K^+ \to \pi^+\nu\bar{\nu})$, measured at BNL by the E949 collaboration
- $\mathcal{B}(K^0_L \to \pi^0\nu\bar{\nu})$, to be measured at BNL by the KOPIO collaboration

Thus, measurements in the K system, in addition to measuring V_{td} independently of $\Delta m_s/\Delta m_d$, allow a comparison of CP violation in the K and B systems. An inconsistency between these measurements could be an indication of non-Standard Model physics.

The small uncertainty ($\sim 7\%$) in the theoretical calculation of $K^+ \to \pi^+\nu\bar{\nu}$ is a result of

- the small magnitude of long-distance effects, $\sim O(10^{-13})$
- the hadronic matrix element being measurable in the isospin analog reaction $K^+ \to \pi^0 e^+ \nu_e$

The present Standard Model prediction for the branching ratio is $(0.78 \pm 0.11) \times 10^{-10}$.[2–4]

2. Experimental considerations

A schematic diagram of the E949 detector is shown in Fig. 3[5]. Kaons entering from the left in a) are distinguished from pions[2] by an upstream Čerenkov detector and slowed in the BeO/active degrader, passing through beam hodoscope B4 to enter and stop in the scintillating fibre target. Upstream wire chambers (BWPC; not shown) detect multiple particles entering the target simultaneously. The charged decay products exiting the target traverse the inner trigger counters ("I-counters"), pass through the low-mass drift chamber, and into a cylindrical range-stack (RS), all immersed in a 1-T magnetic field. The position measurement in the RS is augmented by 2 sets of straw chambers (RSSC). A 4π calorimeter whose main components are a lead/scintillator barrel veto and undoped CsI crystal endcaps provides photon vetoing. Because of the extremely

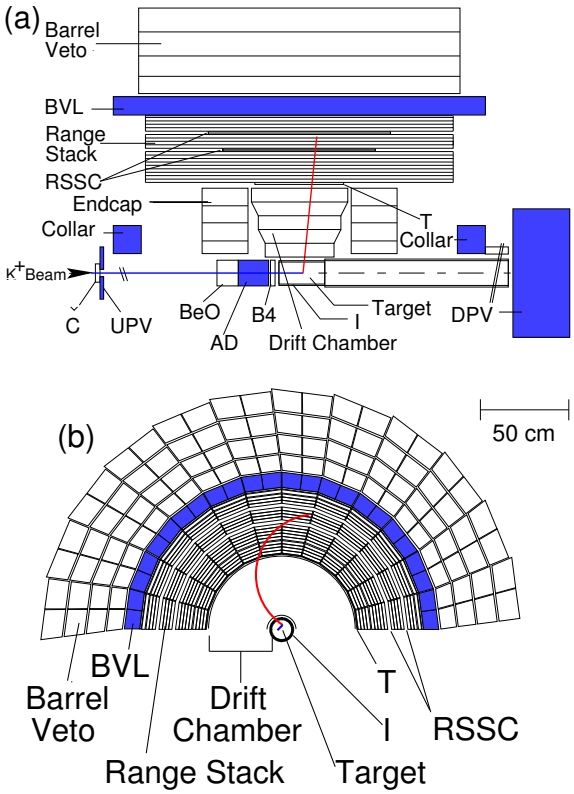

Figure 3. E949 detector schematic diagram. a) side view b) end view

low expected branching ratio, and the distinct lack of distinction of the experimental signature—a single π^+ from a 3-body decay with $p_{\pi^+} < 227\,\mathrm{MeV}/c$—the detection strategy aims at as complete a measurement of the entire decay as possible, including:

- Positive i.d. of single K^+ entering, stopping, and decaying in target
  - Particle i.d. (Čerenkov, B4 hodoscope dE/dx) upstream of target
  - Scintillating fiber target for energy, time, and stopping position measurement
  - "Delayed coincidence" (DELCO) between K^+ stop, and subsequent detection of outgoing particle

[2]The beam has a typical K^+/π^+ ratio of $\sim 4:1$.

- Positive i.d. of decay particle
  - Precise momentum measurement
  - Tracking in range stack: measure total energy and range (with target and I-counters)
  - Observe complete $\pi \to \mu \to e$ decay in stopping counter with 500 MHz Transient Digitizers
- Veto energy *not* associated with $K \to \pi \to \mu \to e$ decay chain
  - Look for extra particles entering the target (B4, BWPC, Čerenkov)
  - Look for photon, neutron energy at K^+ decay time, and accidental hits around stopping counter at π^+ decay time

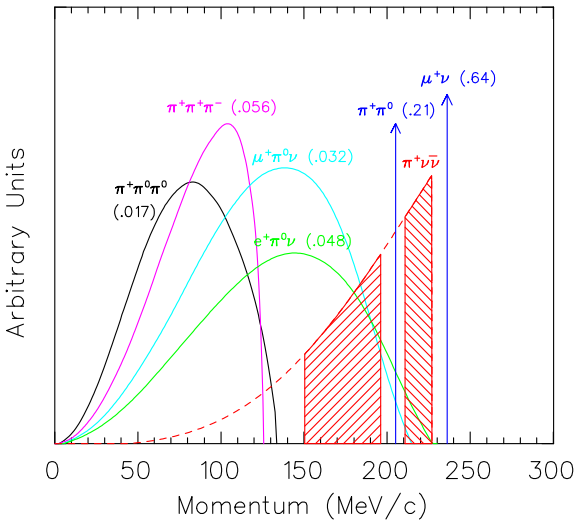

Figure 4. Principal backgrounds to $K^+ \to \pi^+\nu\bar{\nu}$ from K^+ decays.

3. Backgrounds

Fig. 4 shows the major backgrounds to $K^+ \to \pi^+\nu\bar{\nu}$ due to other K^+ decays. In this analysis the phase space is limited to momenta in the range $211\,\mathrm{MeV}/c < p_{\pi^+} < 229\,\mathrm{MeV}/c$; here, only the 2-body $K^+ \to \pi^+\pi^0$ ("$K_{\pi 2}$") and $K^+ \to \mu^+\nu_\mu$ ("$K_{\mu 2}$") decays, and to a lesser degree radiative $K_{\mu 2}$ and $K^+ \to \mu^+\nu_\mu\pi^0$ decays, contribute significantly. Other non-negligible backgrounds come from pions scattered from the beam, and K^+ charge exchange reactions followed by $K_L^0 \to \pi^+ l^- \overline{\nu}_l$, where $l = e$ or μ. Background suppression in the momentum region below the $K_{\pi 2}$ peak is complicated (and dominated) by $K_{\pi 2}$ events in which the π^+ scatters inelastically in the target, coupled with the photons from the π^0 escaping at small angles relative to the beam direction, where the rejection of γ's by the photon veto is lower.

4. Analysis

4.1. Background measurement

Background supression is based on applying two sets of independent selection criteria ("cuts") to each background type. For example, $K_{\pi 2}$ decays are supressed by kinematic cuts (*i.e.* staying away from the $K_{\pi 2}$ peak in total momemntum, energy, and range), and by the photon veto cuts; $K_{\mu 2}$ decays are suppressed by kinematic cuts (chiefly, the consistency of the momentum, energy, and range with a pion hypothesis), and by demanding the positive identification of the complete $\pi^+ \to \mu^+ \to e^+$ decay chain.

Using two sets complementary cuts also serves to make the analysis of the signal region "blind", since the background rejection for one set of cuts is measured with the other set of cuts inverted to insure that the signal region is not examined prior to the completion of all of the background estimates.

To insure that the background estimates themselves are unbiased, the cuts are developed and set on a uniformly-sampled 1/3 portion of the data, and the background levels measured on the remaining 2/3 portion.

The backgrounds are set to the desired levels by adjusting the severity of the cuts. The resulting sets of background predictions as a function of cut severity serves two purposes:

1. Simultaneously reducing the severity of both sets of cuts relative to the values which defined the signal region produced a testable prediction outside the signal region.

2. Insuring that all sets of cuts had some "extra rejection"—again, relative to the values which defined the signal region—resulted in unbiased functions for evaluating any candidate events that may be found when the signal region was finally examined.

4.2. Likelihood analysis

Within the limits dictated by the useful range of the background functions, the level of background chosen depends on how the signal region will be evaluated. Previous analyses[6] used what is commonly referred to as the "cut and count" method. With this method, the total background level was forced to be very low (< 0.1 events), and the branching ratio limits depended only on the the total number of candidate events in the signal region. The drawbacks of this method are that it does not take full advantage of all of the available information about the candidate events (*i.e.* the more detailed knowledge of backgrounds and signal acceptance in various subregions of the designated signal region); it is difficult to assess systematic uncertainties affecting the background and acceptance measurements; it is difficult combine results from different measurements.

The likelihood analysis uses the detailed measurements of background and acceptance described in the previous section to subdivide the signal region into many smaller regions; each candidate event is localized to a particular multi-dimensional "cell" within the global signal region, each dimension of the cell corresponding to one of the background functions. The cells used in this analysis are 7-dimensional. Every background function has a corresponding signal acceptance function; thus, every cell has a total background volume, as well as a total signal acceptance volume. The most important property of each cell is the ratio of total signal acceptance to total background, since this determines how signal- or background-like each candidate event is, and hence how much weight that candidate event carries in the branching ratio determination.

Because the weights of potential candidate events are properly accounted for in the likelihood analysis, the signal region can be expanded to increase the signal acceptance without worrying that a potential background-like candidate event will cause a mismeasurement of the branching ratio.

4.3. Confidence limit determination

The determination of the branching level confidence limits uses the method described in [7]. An optimal "test statistic", X, is defined as the Poisson likelihood ratio:

$$X = \prod_{i=1}^{M} X_i \tag{1}$$

$$X_i = \frac{e^{-(s_i+b_i)}(s_i+b_i)^{d_i}}{d_i!} \Big/ \frac{e^{-b_i} b_i^{d_i}}{d_i!} \tag{2}$$

$$= e^{-s_i}\left(1+\frac{s_i}{b_i}\right)^{d_i} \tag{3}$$

where b_i, s_i, and d_i are the expected background, signal, and number of observed events, respectively, in each cell. Next, the Poisson probabilities for $s+b$, and b only

$$P_{s+b} = \prod_{i=1}^{M} P_{s+b}(d_i; s_i+b_i) \tag{4}$$

$$= \prod_{i=1}^{M} \frac{e^{-(s_i+b_i)}(s_i+b_i)^{d_i}}{d_i!} \tag{5}$$

$$P_b = \prod_{i=1}^{M} P_b(d_i; b_i) \tag{6}$$

$$= \prod_{i=1}^{M} \frac{e^{-b_i} b_i^{d_i}}{d_i!} \tag{7}$$

are calculated, and summed over all values of $X < X_{\text{observed}}$ to give the corresponding $s+b$, and b-only confidence limits:

$$CL_{s+b} = P_{s+b}(X \le X_{\text{observed}}) \tag{8}$$

$$= \sum_{X(\{d'_i\}) \le X(\{d_i\})} \prod_{i=1}^{n} \frac{e^{-(s_i+b_i)}(s_i+b_i)^{d'_i}}{d'_i!} \tag{9}$$

$$CL_b = P_b(X \le X_{\text{observed}}) \tag{10}$$

$$= \sum_{X(\{d'_i\}) \le X(\{d_i\})} \prod_{i=1}^{n} \frac{e^{-(b_i)}(b_i)^{d'_i}}{d'_i!} \tag{11}$$

The "Modified frequentist" confidence level is

then taken as the ratio

$$CL_s = CL_{s+b}/CL_b \quad (12)$$

A complete set of confidence levels are thus derived by scanning over different assumed levels of expected signal, *i.e.* by varying a multiplicative factor applied to s; the central value of the branching ratio—assuming that candidate events are found—is *defined* to be at that value of the branching ratio that maximizes X_{observed}. Although different definitions for the central value are possible (e.g. the median (50%) confidence level) the definition used has been chosen because of certain desirable properties with respect to the asymptotic values of the candidate cell s/b values:

- For high values of s/b the central value approaches the "classic" definition of a branching ratio, namely the product of the number of candidate events and the single event sensitivity;
- Assuming the combination of the new data with a previously measured data set with a non-zero central value branching ratio, for low values of s/b the combined central value and lower/upper confidence approaches what they would be if no new candidate events were found in the new data.

5. Results

5.1. Background levels and sensitivity

Table 5.1 shows the background levels inside the signal region for the 2002 data set. As described above, the total background level has been deliberately increased compared with previous analyses in order to gain more signal acceptance. Table 2 gives a comparison of the number of stopped K^+'s, the total acceptance, and the total background for the combined E787 data sets[6] and the E949 2002 data set[8].

5.2. Signal region examination

The signal region for the 2002 data set contained a single candidate event. The background functions described in Section 4.1 indicate that the new candidate event has a higher *a priori* probability of being a background event then either of the two previous E787 candidate events,

Background	Events
$K_{\pi 2}$	0.216 ± 0.023
$K_{\mu 2}$	0.044 ± 0.005
$K_{\mu m}$	0.024 ± 0.010
1-beam	0.006 ± 0.002
2-beam	0.003 ± 0.002
CEX	0.005 ± 0.001
Total	0.298 ± 0.026

Table 1
Background levels for the 2002 data set. "$K_{\mu m}$" refers to multi-body backgrounds with contributions from $K^+ \to \mu^+\nu\gamma$, $K^+ \to \mu^+\pi^0\nu$, and $K_{\pi 2}$ with $\pi^+ \to \mu^+\nu$ decay-in-flight; "1-beam" to scattered pions; "2-beam" to events with more than 1 beam particle entering the detector; "CEX" to K^+ charge exchange.

	E787	E949
# K^+	5.9×10^{12}	1.8×10^{12}
Acceptance	0.0020 ± 0.0002	0.0022 ± 0.0002
Background	0.14 ± 0.05	0.30 ± 0.03

Table 2
Comparison of number of stopped kaons, total acceptance, and total background for the combined data sets of E787[6] and the 2002 data set of E949.[8]

owing chiefly to its small measured π^+ lifetime of 6.2 ns and its momentum of $227.3 \pm 2.7\,\text{MeV}/c$. Nonetheless, all of its properties including, these two, are also consistent with being a signal event. Table 3 shows the results of the likelihood analysis for the combined E787 and E949 data sets, including the signal-to-background ratios (s_i/b_i) at the measured branching ratio, and the weights (W_i) of the candidate events in the branching ratio determination. Also shown on the bottom line are the a priori background probabilities ($1-CL_b$) for the candidates, *i.e.* the probability that background processes alone would have produced candidate configurations as or more signal-like than the observed configurations within their respective data sets.

	E787		E949
Candidate	1995A	1998C	2002A
s_i/b_i	50	7	0.9
$W_i \equiv s_i/(s_i+b_i)$	0.98	0.88	0.48
$1-CL_b$	0.006	0.02	0.07

Table 3
Characteristics of E787 and E949 $K^+ \to \pi^+\nu\bar{\nu}$ candidate events. See text for details.

5.3. Branching ratio and confidence limits

The branching ratio and confidence limits for the combined E787 and E949 2002 data sets are obtained as described in Sec. 4.3. Fig. 5 shows the results of that scan, leading to the recently published result[8] of

$$\mathcal{B}(K^+ \to \pi^+\nu\bar{\nu}) = (1.47^{+1.30}_{-0.89}) \times 10^{-10}$$

The top plot shows X_{observed} as a function of the branching ratio, which is obtained by applying a variable multiplicative factor proportional to the signal acceptance to the single event sensitivity. The maximum value of X_{observed} is taken as the central value of the branching ratio. The bottom plot shows the signal confidence level CL_s as a function of the branching ratio. The 68% confidence interval quoted in [8] is taken from the lower and upper 16% confidence levels as read from this plot.

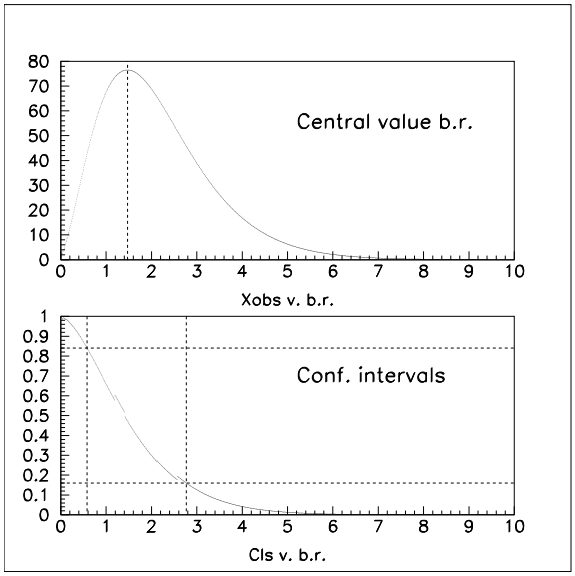

Figure 5. Determination of the central value branching ratio (top) and the 68% confidence interval for the combined E787 and E949 data sets.

6. Summary

The E949 collaboration has used the measured value of $\mathcal{B}(K^+ \to \pi^+\nu\bar{\nu})$ by combining the 2002 data set with the previous E787 results. The experimental and analytical challenges posed by this extremely difficult measurement have been met through a variety of innovative techniques. Steady improvements to both the detector and the analysis method have been made with each new data set.

REFERENCES

1. L. Wolfenstein, Phys. Rev. Lett. 51, 1945 (1983).
2. G. Buchalla and A. J. Buras, Nucl. Phys. **B548** 309 (1999).
3. G. Isidori, eConf **C0304052**, WG304 (2003)[arXiv:hep-ph/0307014] and references therein.
4. A. J. Buras, hep-ph/0402112 (2004).
5. M.S. Atiya *et al.*, Nucl. Instr. Meth. **A321**, 129 (1992); I-H. Chiang *et al.*, IEEE Trans. Nucl. Sci. **NS-42**, 394 (1995); D.A. Bryman *et al.*, Nucl. Instr. Meth. **A396**, 394 (1997); E.W. Blackmore *et al.*, Nucl. Instr. Meth. **A404**, 295 (1998); T.K. Komatsubara *et al.*, Nucl. Instr. Meth. **A404**, 315 (1998).
6. S. Adler *et al.*, Phys. Rev. Lett. **88**, 041803 (2002); S. Adler *et al.*, Phys. Rev. Lett. **84**, 3768 (2000); S. Adler *et al.*, Phys. Rev. Lett. **79**, 2204 (1997).
7. T. Junk, Nucl. Instr. Meth. **A434**, 435 (1999).
8. V.V. Anisimovsky *et al.* Phys. Rev. Lett. **93**, 031801.